Chemical Technology, Control and Management

Volume 2018
Issue 3 *SPECIAL ISSUE 4-5*

Article 25

10-19-2018

Method for diagnostic of permanent-magnet electrical machines.

F.R Ismagilov
Department of Electromechanics, Ufa State Aviation Technical University, Russian Federation, Address: Ul. K. Marxa 12, Ufa, the Republic of Bashkortostan, Russian Federation, 450008

V.Ye Vavilov
Department of Electromechanics, Ufa State Aviation Technical University, Russian Federation, Address: Ul. K. Marxa 12, Ufa, the Republic of Bashkortostan, Russian Federation, 450008

V.V Ayguzina
Department of Electromechanics, Ufa State Aviation Technical University, Russian Federation, Address: Ul. K. Marxa 12, Ufa, the Republic of Bashkortostan, Russian Federation, 450008, vtipy@mail.ru

Method for diagnostic of permanent-magnet electrical machines.

Cover Page Footnote

Tashkent State Technical University, SSC «UZSTROYMATERIALY», SSC «UZKIMYOSANOAT», JV «SOVPLASTITAL», Agency on Intellectual Property of the Republic of Uzbekistan

Erratum

??????

ISSN 1815-4840
CHEMICAL TECHNOLOGY. CONTROL AND MANAGEMENT
2018, Special issue №4-5 (82-83) pp.113-119
International scientific and technical journal
journal homepage: ijctcm.com
Since 2005

METHOD FOR DIAGNOSTIC OF PERMANENT-MAGNET ELECTRICAL MACHINES

F.R.Ismagilov[1], V.Ye.Vavilov[2], V.V.Ayguzina[3]

[1,2,3] *Department of Electromechanics, Ufa State Aviation Technical University, Russian Federation*
Address: Ul. K. Marxa 12, Ufa, the Republic of Bashkortostan, Russian Federation, 450008
E-mail: [3]vtipy@mail.ru

Abstract: *This paper proves that the use of conventional diagnostic methods of rotor crack and local demagnetization based on the harmonic analysis of the output voltage or back-electromotive force is effective only with a certain ratio of the number of slots and poles. This statement was proved experimentally. The diagnostic method of the rotor cracks and local demagnetization which is universal for all types of windings and the number of slots of 2-pole synchronous electric machines with permanent magnets is proposed. The mathematical apparatus for the implementation of the proposed method is developed and is verified with the help of FEM and experimental studies. All the experimental studies have been carried out for various rotor magnetic systems and a different number of stator slots.*

Keywords: *Crack Detection, Fault Diagnosis, Permanent Magnet Machines, Back-Electromotive Force, Rotor Magnetic System*

Introduction

Permanent-magnet electrical machines (PMEMs) have found wide application in all industries [1]. It is effective solution to design high-speed generators with a rotational speed range from 24,000 to 800,000 rpm due to their high efficiency and controllability [2]. As the PMEMs are used in highly responsible system, it is necessary to predict and diagnose all of their faults in a real time. One of the main faults is a partial demagnetization of permanent magnet (PM) or its mechanical damage. The PM demagnetization can occur in the case of the short circuit or the PM overheating [3]-[4]. PM splits and cracks are a more difficult to determine defect of the PMEM, because it cannot be visually determined. The PM cracks and splits can be insignificant and have almost no effect on voltages and currents of PMEM. However, the rotor mechanical loads will lead to the further PM destruction during the PMEM operation especially in high-speed systems. Another problem is the difficulty to monitor the rotor position. This problem occurs when the Hall sensors are used, which reacts to the rotor magnetic system (RMS).

The use of methods based on the harmonic analysis of the output voltage or back-EMF is effective only with a certain number of slots and poles. It means that diagnostic criteria cannot be extended from the results of one PMEM study to another one with a different number of slots and poles. In addition, a new method for PMEM diagnostic was proposed.

1. Experimental studies of rotor cracks and local demagnetization

Industrial enterprises engaged in the production of high-speed PMEM use mainly 2-pole RMSs in their products due to the minimum losses in the stator magnetic core, and more rarely use 4-pole ones [5]-[6]. Analysis of known diagnostic methods [7]-[10] has shown that the most effective method is one by back-EMF. Its advantages are the ease of implementation and the minimal impact of environmental conditions on its effectiveness. The disadvantage is an inability to analyze a stationary PMEM rotor.

To formulate diagnostic criteria, an experimental study of PMEM with parameters

presented in Table I were carried out. In experimental studies, two 2-pole rotors with and without cracks were considered (Fig. 1). These rotors are intended for use in a 5-kW 96,000-rpm high-speed PMEM. To ensure the possibility of visual rotor monitoring, the rotor sleeve has been removed from them. Tests were performed for a 6-slot PMEM with a tooth-coil winding. For the tooth-coil winding, there are 3 basic configurations (Fig. 2). The topology A (all teeth wound) has a high fill factor. The disadvantage of this one is a low fault tolerance since a short circuit in one phase or in one winding can cause a short circuit in the adjacent winding or the adjacent phase. The topology B (alternate teeth wound) has a low fill factor.

Table 1.

Parameters of the investigated topologies

Parameters	Rated parameters		Experimental data	
	A	B	A	B
Rotational speed, rpm	96000		2800	
Rms-phase voltage, V	51	51	1.5	1.5
Rms-phase current at full load, A	14	14	14	14
Number of poles	2	2	2	2
Active length, mm	50	50	50	50
Outer stator diameter, mm	50	50	50	50
Rotor sleeve thickness, mm	2	2	0	0
Number of turns in phase	20	20	20	20
Resistance of stator winding, Ohm	0.035	0.028	0.035	0.028
Number of stator slots	6	6	6	6
Winding type	Tooth-coil, all teeth wound			
Winding factor	0.5	0.5	0.5	0.5
Stator core material	Amorphous magnetic material 5BDSR with a thickness of 25 μm / 1.3 T			
PM material	SmCo			
PM thickness, mm	5	5	5	5

However, as winding occupies only one slot, a short circuit in one phase does not significantly affect adjacent windings and phases and will not cause a short circuit in them. The topology C (alternate teeth wound Unequal Tooth Width) is a special case of the topology B.

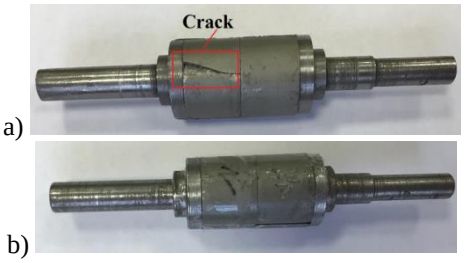

Figure 1. ***The investigated rotors with (a) and without (b) a crack.***

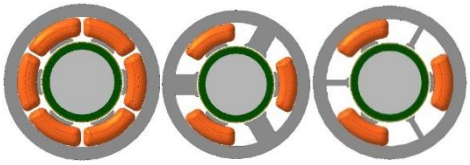

Figure 2. ***PMEM configurations***

Experimental studies were carried out only for topologies A and B. The topology C was not considered since it is a special case of the topology B. All the tests were performed in the generator mode with an active load. Fig. 3 shows the 2-pole PMEM and the stand for its tests. The main task was to evaluate the EMF depending on the rotor defect. The experimental results for a serviceable and defective rotor are shown in Fig. 4.

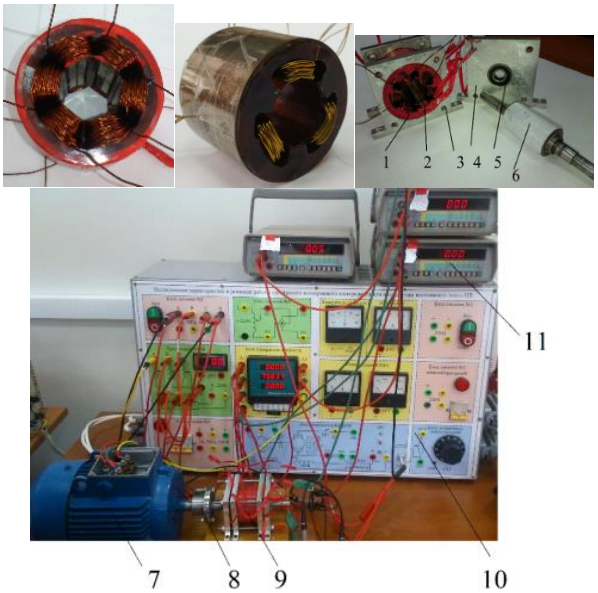

Figure 3. ***PMEM and test stand.***

Here: 1 is a stator magnetic core; 2 is a stator winding; 3 is a housing; 4 is a bearing shield; 5 are bearings; 6 is a rotor; 7 is a drive motor; 8 is a coupling; 9 is a tested layout; 10 are measuring instruments; 11 is a voltmeter

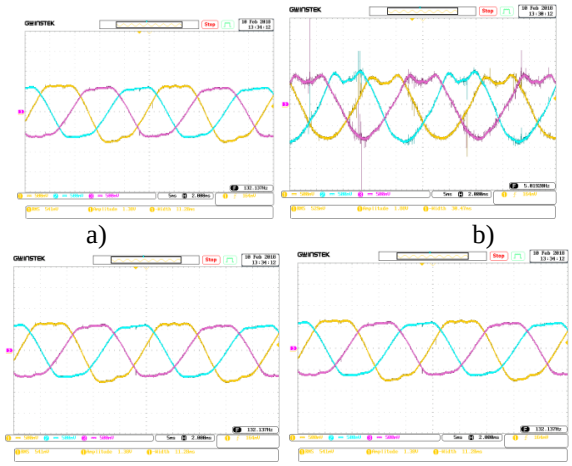

Figure 4. ***Results for the serviceable (a) and defective rotor (b) of the B topology and for the serviceable (c) and defective rotor (d) of the A topology***

For the PMEM with the defective rotor and the tooth-coil winding (alternate teeth wound), the EMF becomes asymmetric with respect to the abscissa axis. A similar EMF form is practically does not occur in electrical machines. The use of a serviceable rotor in this PMEM resulted in the symmetry of the output EMF relative to the abscissa axis. Thus, the diagnostic criterion for one-side PM crack or local demagnetization for a given winding type, number of poles and slots is the asymmetry of the output voltage along the abscissa axis. Similar results were obtained at a full load, which proves that the current in the PMEM windings has practically no effect on the detected diagnostic criteria.

Using the same rotors, experimental studies were carried out on the stator magnetic core with a tooth-coil winding type (all teeth wound). The experimental results are also shown in Fig. 4. It can be seen that for a given winding type and the number of slots, the rotor defect was practically not manifested in the output EMF. This result proves that the use of EMF as a diagnostic criterion is effective only for a certain ratio of the number of slots and poles. Diagnostic criteria cannot be extended from the study results of one PMEM to another with a different number of slots and poles.

Similar studies were also carried out for the other RMS types (Fig. 5). The results was the same in all cases.

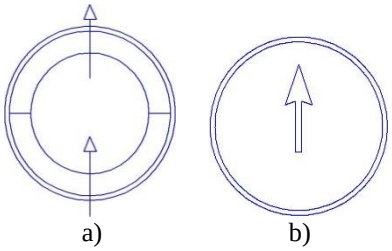

Figure 5. ***a) RMS with semicircular PM; b) RMS with cylindrical PM***

A diagnostic method for the rotor crack and local PM demagnetization for a 2-pole PMEM was proposed, in which an additional three-phase alternating teeth wound is used. This winding can have a minimum number of turns and practically do not increase the mass and overall dimensions of PMEM. The diagnostic winding should consist of three coils, each of which is a phase. In this case, the coils are located symmetrically in the three slot, regardless of the number of stator slots. The EMF is measured from this winding and, according to the symmetry or asymmetry of this EMF, a conclusion about the technical condition of the 2-pole rotor relative to the abscissas axis is drawn. It is important to note that neither environmental conditions nor the currents induced in the PMEM windings will affect the diagnostic criteria. In addition, the proposed method does not require decomposing the output EMF in a Fourier series; its implementation requires only a comparison of several EMF values at certain points of time. The drawback of this method is that it does not allow to carry out diagnostics of PMs with a stationary rotor; and also this method is most effective at one-sided rotor local demagnetization.

2. Mathematical description of the PMEM magnetic field at PM local demagnetization

The pole crack or local demagnetization will lead to a decrease in the magnetic flux density on the PM surface and a change in the PM magnetization amplitude. To understand this process, it seems reasonable to consider its mathematical description. The calculation scheme

with the magnetic flux density lines distribution is shown in Fig. 6.

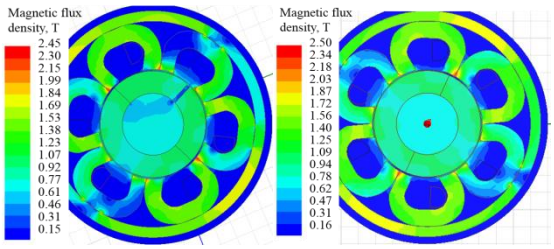

Figure 6. ***Magnetic flux density distribution of the PMEM with defective (a) and non-defective (b) rotors***

In the PM local demagnetization analysis, the following assumptions were used:

- As the EMF for diagnostic is idling and obtained from an additional winding, the idling magnetic field is considered.
- The 2-pole RMS is considered.
- The magnetic steel permeability of a core and a shaft is equal to infinity; the magnetic permeability of the air gap is equal to the magnetic permeability of vacuum.
- The axial component of the magnetic field strength in the end rotor surfaces is equal to 0, i.e. the PMEM with infinite length is considered.
- The winding is presented as a thin copper layer; the current density vector contains only the axial component.
- Eddy currents in PMs and the rotor sleeve are not taken into account.
- The magnetic field on the PM surface is specified as a normal component of the magnetic flux density harmonic series [11].

To analyze the magnetic field, the Maxwell equations were used [12]. Since the local PM demagnetization should be manifested in both load modes, it is advisable to consider the idling mode. The Laplace equation in cylindrical coordinates was considered. The boundary conditions will be the normal component of the magnetic flux density given on the surface and equation $H_\varphi \mid_{r=\frac{D_{pm}+2\delta}{2}} = 0$.

The solution for the tangential component of the magnetic field in the air gap is follows:

$$H_\varphi = \frac{A_0}{2}\frac{R_0^{\left(\frac{D_{PM}}{2}\right)}(r)}{R_0^{\left(\frac{D_{PM}}{2}\right)}\left(\frac{D_{PM}+2\delta}{2}\right)} + \sum_{n=1}^{\infty}\frac{R_n^{\left(\frac{D_{PM}}{2}+\delta\right)}(r)}{R_n^{\left(\frac{D_{PM}}{2}+\delta\right)}\left(\frac{D_{PM}}{2}\right)}\{A_n\cos n\varphi + B_n\sin n\varphi\}, \quad (1)$$

where $r = \frac{D_{PM}}{2}$ is a PM radius; D_{PM} is a PM diameter; $R_n^{\left(\frac{D_{PM}}{2}+\delta\right)}(r) = \frac{-r^{2n}+\left(\frac{D_{PM}+2\delta}{2}\right)}{r^n}$; $R_0^{\left(\frac{D_{PM}}{2}\right)}(r) = \ln\frac{2r}{D_{PM}}$; A_0, A_n, B_n are the constant components, determined from the boundary conditions.

The following designation is introduced: $\frac{D_{PM1}+2\delta}{2} = R_S$, $\frac{D_{PM}}{2} = R_{PM}$.

Equation (1) is rewritten as follows:

$$H_\varphi = \frac{A_0}{2}\frac{R_0^{(R_{PM})}(r)}{R_0^{(R_{PM})}(R_s)} + \sum_{n=1}^{\infty}\frac{R_n^{(R_S)}(r)}{R_n^{(R_S)}(R_{PM})}\{A_n\cos n\varphi + B_n\sin n\varphi\}. \quad (2)$$

A local demagnetization of the rotor section into the mathematical description of the PMEM magnetic field is introduced. With a PM local demagnetization, the normal component of the magnetic field on the PM surface will drop out of the harmonic Fourier series. For $r = \frac{D_{PM}}{2}$, there is follows:

$$r = \frac{D_{PM}}{2}\quad B_r(\varphi) = \sum_{n=1}^{\infty} B_{rn\max}\cos n\varphi;$$
$$B_{rn\max} = \frac{2}{\pi}\int_{-\frac{\pi}{2}}^{\frac{\pi}{2}} B_M\cos^2 n\varphi d\varphi, \quad (3)$$

besides $\varphi=\gamma$. For $\varphi=\gamma$, B_M is greater or equal to 0 but smaller for other φ values. Angle γ characterizes the PM local demagnetization coordinate. The PM local demagnetization along the radius was not characterized.

For $r = R_s$, there is follows:

$$R_0^{(R_{PM})}(r)=\ln\left(1+\frac{\delta}{D_{PM}}\right),\quad R_0^{(R_{PM})}(R_s)=\ln\left(1+\frac{\delta}{D_{PM}}\right),$$

$$R_n^{(R_{PM})}(r)=\frac{R_s^{2n}-R_{PM}^{2n}}{R_s^n},\quad R_n^{(R_{PM})}(R_s)=\frac{R_s^{2n}-R_{PM}^{2n}}{R_s^n},$$

$$\frac{A_0}{2}+A_n\cos n\varphi+B_n\sin n\varphi=\sum_{n=1}^{\infty}B_{rn\max}\cos n\varphi,$$

$$B_{rn\max}=\frac{2}{\pi}\int_{-\frac{\pi}{2}}^{\frac{\pi}{2}}B_M\cos^2 n\varphi\,d\varphi, \qquad (4)$$

besides $\varphi=\gamma$. For $\varphi=\gamma$, B_M is greater or equal to 0 but smaller for other φ values. Then:

$$A_0=0,\ B_n=0,\ \sum_{n=1}^{\infty}A_n\cos n\varphi=\sum_{n=1}^{\infty}B_{rn\max}\cos n\varphi. \qquad (5)$$

Tangential and radial components of the flux density in the air gap are follows:

$$B_r(r,\varphi)=\sum_{n=1}^{\infty}B_{rn\max}\frac{R_{PM}}{r}\frac{\left(\frac{r}{R_s}\right)^n+\left(\frac{R_s}{r}\right)^n}{\left(\frac{R_{PM}}{R_s}\right)^n+\left(\frac{R_s}{R_{PM}}\right)^n}\cos n\varphi, \qquad (6)$$

$$B_\varphi(r,\varphi)=\sum_{n=1}^{\infty}B_{rn\max}\frac{R_{PM}}{r}\frac{\left(\frac{r}{R_s}\right)^n-\left(\frac{R_s}{r}\right)^n}{\left(\frac{R_{PM}}{R_s}\right)^n+\left(\frac{R_s}{R_{PM}}\right)^n}\sin n\varphi, \qquad (7)$$

besides $\varphi=\gamma$. For $\varphi=\gamma$, $B_{rn\max}$ is greater or equal to 0, but smaller for other φ values.

The obtained equations allow to determine the magnetic flux density in the air gap for various PM local demagnetizations.

Fig. 6 shows that the magnetic flux density is not distorted significantly. The rotor crack does not lead to an asymmetry flux density in the stator core. Therefore, mechanical crack or local demagnetization does not occur in all the winding types. The three-phase winding consisting of three coils is the cause of asymmetric magnetic fields. Therefore, even a non-significant asymmetry of the magnetic field is significantly reflected in its EMF. Computer simulation results are presented in Fig. 7. The PM crack was simulated by introducing a slight air gap between the PMs. The angular coordinate of the gap was 45º. The stator core saturation was not taken into account in computer simulation. The discrepancy between analytical and FEM results is below 7 %. A comparison of the experimental results, modeling and analytical calculations with the non-defective rotor in Figs. 7a and 4a show that the EMF is different. It was caused by the stator core saturation, which was not considered in analytical and computer models. The numerical discrepancy between the analytical calculations, computer modeling and experimental results was below 10 %.

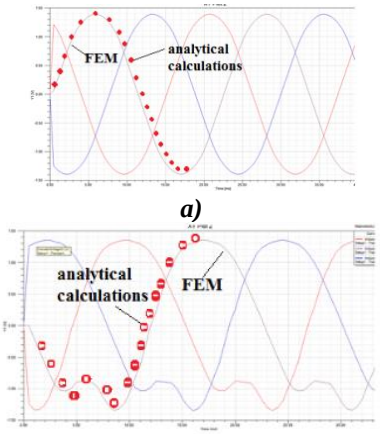

Figure 7. ***Computer simulation results for the serviceable (a) and defective rotors (b)***

3. Experimental studies of the diagnostic method for PM local demagnetization for different RMSs

To evaluate the effectiveness of the proposed method, 4 experimental PMEM samples were created. The samples had a different number of slots, various RMSs, and various stator geometric dimensions (Fig. 5). Rotor with RMS A is shown in Fig. 1. The RMS B is shown in Fig. 8.

All tests were performed in the generator mode on the stand shown in Fig. 3. Table 2 and Fig. 8 show the characteristics and appearance of the prototype with the distributed winding. The prototype is shown in Fig. 3. In each prototype, an inoperative rotor with a magnetic system A and B was installed and a special measuring three-phase alternating teeth wound winding was placed on the stator of each of the prototypes. The back-EMF was measured from the main winding and from the diagnostic winding. The measuring winding consisted of three coils, each of which is a phase. Coils were located symmetrically in the three slots, regardless of the number of slots of the stator core.

Figure 8. ***The 18-slots PMEM with RMS B***

Table 2.

Characteristics of the experimental models

Prototype	A	B	C	D
Type of stator winding	Distrib uted	Tooth-coil	Distrib uted	Tooth-coil
Number of stator slots	18	6	18	6
Rotational speed, rpm	2800	2800	2800	2800
Outer stator diameter, mm	65	60	65	60
Inner stator diameter, mm	40	32	40	32
Outer rotor diameter	25	25	28	28
Active stator length, mm	50	50	50	50

The experimental results are shown in Fig. 9. The experimental results for topology B are similar to those shown in Fig. 7. The results for topology D are analogous to the results of topology C. Therefore, results for these topologies are not presented.

Experimental results show that there are no disturbances on the back-EMF of the main winding with a faulty rotor. The EMF of the measuring winding has significant distortion and asymmetry relative to the abscissa axis regardless of the RMS type. Thus, the experimental results of various geometric dimensions and parameters of PMEM unequivocally confirm the efficiency and workability of the proposed method and prove the possibility of using it for all 2-pole RMS and for any number of slots. In addition, a discrepancy between the proposed analytical and computer models with experimental data does not exceed 10 %, therefore the developed models can be used in practice.

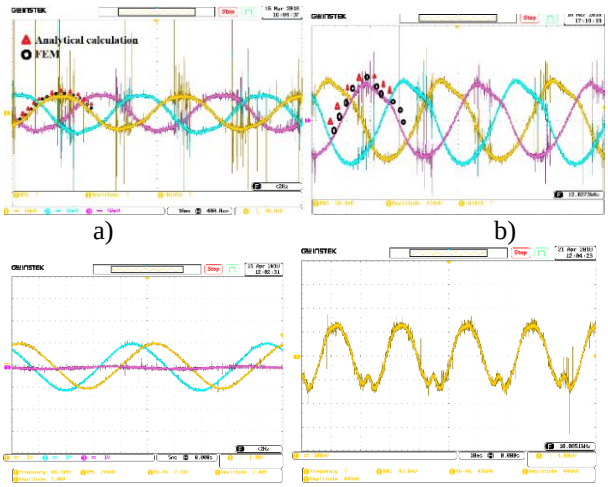

Figure 9. ***Experimental results: a) topology C, back-EMF of the main winding; b) topology C, back-EMF of measuring winding; c) topology D, back-EMF of the main winding; d) topology D, back-EMF of measuring winding***

Conclusion

The effect of rotor cracks and local demagnetization on the characteristics of the 6-slot 2-pole PMEM with a tooth-coil winding were investigated. It was found that the use of methods based on the harmonic analysis of the output voltage or back-EMF is effective only with a certain ratio of the number of slots and poles. Based on the experimental studies, the diagnostic method of the rotor cracks and local demagnetization was developed, which is universal for all types of windings and the number of slots of 2-pole PMEMs. The mathematical apparatus for the implementation of the proposed method was presented.

All experimental studies have been carried out for various rotor magnetic systems and a different number of stator slots. This allowed to confirm the effectiveness of the proposed method.

REFERENCES

1. Borisavljevic A., Polinder H., Ferreira J., “On the Speed Limits of Permanent-Magnet Machines,” IEEE Transactions on Industrial Electronics, vol. 57, no. 1, pp. 220–227, 2010.
2. Ganev E., “Selecting the Best Electric Machines for Electrical Power-Generation Systems: High-performance solutions for aerospace More electric architectures,” IEEE Electrification Magazine, vol. 2, no. 3, pp. 13-22, Dec. 2014.

3. Liu K., Zhu Z.Q., "Online Estimation of Rotor Flux Linkage and Voltage Source Inverter Nonlinearity in Permanent Magnet Synchronous Machine Drives," IEEE Transactions on Power Electronics, vol. 29, no. 1, pp. 418–427, Jan. 2014.
4. Vinson G., Combacau M., Prado T., Ribot P., "Permanent Magnets Synchronous Machines Fault Detection and Identification," IECON 2012 - 38th Annual Conference on IEEE Industrial Electronics Society, pp. 3925-3930, Oct. 2012.
5. Borisavljevic A., Limits, Modeling and Design of High-Speed Permanent Magnet Machines, Springer-Verlag Berlin Heidelberg, 218 p., 2013.
6. Uzhegov N., Kurvinen E., Nerg J., Sopanen J.T., Shirinskii S., "Multidisciplinary Design Process of a 6-Slot 2-Pole High-Speed Permanent-Magnet Synchronous Machine," IEEE Transactions on Industrial Electronics, vol. 63, no. 2, Feb. 2016.
7. Liu K., Zhu Z.Q., Stone D.A., "Parameter Estimation for Condition Monitoring of PMSM Stator Winding and Rotor Permanent Magnets," IEEE Transactions on Industrial Electronics, vol. 60, no. 12, pp. 5902–5913, Dec. 2013.
8. Jabbar M.A., Dong J., Liu Z., "Determination of machine parameters for internal permanent magnet synchronous motors," Second International Conference on Power Electronics, Machines and Drives, vol. 2, pp. 805–810, 2004.
9. Underwood S., Husain I., "Online Parameter Estimation and Adaptive Control of Permanent-Magnet Synchronous Machines," IEEE Transactions on Industrial Electronics, vol. 57, no. 7, pp. 2435–2443, Jul. 2010.
10. Uresty J.C., Riba J.R., Romeral L., "A Back-emf Based Method to Detect Magnet Failures in PMSMs," IEEE Transactions on Magnetics, vol. 49, no. 1, pp. 591–598, Jan. 2013.
11. Ismagilov F.R., Vavilov V.Y., Miniyarov A.H., Veselov A.M., Ayguzina V.V., "Design, optimization and initial testing of a high-speed 5-kw permanent magnet generator for aerospace application," Progress In Electromagnetics Research C, vol. 79, pp. 225-240, 2017.

Ledovsky A.N., Electric Machines with High-Coercivity Permanent Magnets, Moscow, Energoatomizdat, 169 p., 1985.